RSC Advances

PAPER

View Article Online
View Journal | View Issue

Cite this: *RSC Adv.*, 2022, **12**, 8102

A rational synthesis of ultrasmall palladium-based alloys with superhydrophilicity as biocompatible agents and recyclable catalysts†

Shiyue Chen,‡[ab] Xiaoxiao He,‡[ab] Xulei Yuan,‡[cd] Zhenyu Wang,[ab] Teng Wang,[ab] Chengdian He,[ab] Ximu Zhang[cd] and Xiang Mao *[ab]

Received 14th January 2022
Accepted 28th February 2022

DOI: 10.1039/d2ra00266c

rsc.li/rsc-advances

As essential controlling parameters, the local surface area (size distribution) and polarity property of the surface molecules can determine the catalytic activity and biocompatibility directly. Here, ultrasmall palladium-based alloys (FePd, FePdCo, and FePdCu NCs) were developed to serve as artificial degradation catalysts with superhydrophilicity (SPh), biocompatibility, and reusability, which were referred to as "biocatalysts". As synthesized in aqueous solvent with negative surface potential while dispersing in water medium, because of the surface biological molecules effect. The obtained alloys illustrated a size distribution of about 3.5 nm. Additionally, owing to SPh property, these alloys could be stored in water up to 30 days without any precipitation and retained their monodisperse morphology in colloidal solutions. The cytotoxicity assessment of the alloys by exposing to L-929 cells over 3 days indicated that it maintained cell viability of >80% even up to 390 μg mL^{-1} (concentration of alloys). Furthermore, they exhibited an obvious enhancement in the catalytic performance for degrading Rhodamine B (RhB) and 4-nitrophenol (4-NP). The recyclable utilization of biocatalysts demonstrates durable stability even after 8 reduction cycles.

Owing to their use in different applications, palladium-based alloys have attracted increasing attention due to their excellent physical, chemical, and other characterizations, particularly, in can be deleted synthesis approaches, such as construction of dumbbell structures, core shell structures, and yolk@shell structures.[1] As for palladium-based composites, they exhibit excellent chemical catalytic activity and environmental friendliness. In order to fit the different requirements, synthesis approaches for palladium-based alloys have been well explored, in which, the obtained alloys with different elemental compositions and hydrophobic characteristics showed high energy consumption.[2] Ascribed to the traditional approaches, a palladium-based heterogeneous structure can be realized *via* physical deposition formation (casting alloys)[3] and solvothermal approaches. According to essential initial requirement, particle parameters (size distribution, surface energy) of an ultra-small particle could promote size minimization and enhance surface free energy in order to keep the NCs in a "boiling state". It could enhance the relative performance in the form of biocatalysts. Therefore, it causes poor stability, leading to aggregation and loss of catalytic performance under extreme conditions.[4] In existing requirements, the status of its surface, size distribution and uniformity are subjected to synthetic method in designing scopes. In addition, the hydrophobic surface implies a high possibility of further modifications, which means that alloys might be utilized in biocompatible fields. According to comprehensive procedures for preparing functional biocatalysts, it can be synthesized *via* solvothermal or wet-chemistry approaches. The hydrophobic surface was made up of long chain alkanes and would become hydrophilic using the ligand exchange strategy in surface modification. This process frequently uses hydrophilic molecules or polymers for 'secondary' modification, and particles could achieve a novel surface for specific purposes, such as in electrocatalysis and biocatalysis.[5]

However, the most essential factor in the synthesis is designing a simple synthesized approach to fabricate ultrasmall and superhydrophilic (SPh) biocatalysts with low energy consumption at room temperature (RT). The synthesized ultrasmall alloys showed excellent catalytic activity and environment-friendly characteristics. In order to ensure the

[a]*State Key Laboratory of Ultrasound in Medicine and Engineering, College of Biomedical Engineering, Chongqing Medical University, Chongqing, 400016, P. R. China*

[b]*Chongqing Key Laboratory of Biomedical Engineering, College of Biomedical Engineering, Chongqing Medical University, Chongqing, 400016, P. R. China*

[c]*Chongqing Key Laboratory of Oral Disease and Biomedical Sciences, Stomatological Hospital of Chongqing Medical University, Chongqing, 401174, P. R. China*

[d]*Chongqing Municipal Key Laboratory of Oral Biomedical Engineering of Higher Education, Stomatological Hospital of Chongqing Medical University, Chongqing, 401174, P. R. China*

† Electronic supplementary information (ESI) available. See DOI: 10.1039/d2ra00266c

‡ These authors contributed equally.

ultrasmall and SPh characteristics, it is necessary to promote the possibility of combining one or two metal compositions with palladium element through low energy consuming procedures. The obtained palladium-based alloys could meet the requirements of biocatalysts. Ascribed to the chemical potential of different metal ions, Pd (2.20 eV) possessed much higher electronegativity than Fe (1.83 eV), Co (0.24 eV) and Cu (0.34 eV). The formation of alloyed NCs could enable electron transfer between Pd and other elements involved in the hybridization finally. As prepared in solvent thermography process, palladium-based alloyed biocatalysts can be designed and fabricated successfully.

Herein, a one-step approach has been introduced to prepare uniformly dispersed SPh biocatalysts, such as bimetallic FePd alloy and ternary FePdCo and FePdCu alloy, respectively. Eventually, we established a feasible approach by coupling metal elements in forming biocatalysts. Fig. 1 shows the mechanism of the synthesis approach, in which the solvent medium was a 1 : 1 mixture of H_2O and C_2H_5OH for adjusting polarity. The reaction was carried out significantly with different features from that in an organic solvent, which has been extensively studied for the synthesis of metal-based hydrophobic alloys.[6] Also, the catalytic properties and biocompatibility NCs were referred as biocatalysts, which were extensively investigated, and their catalytic properties in the degradation during treatment with Rhodamine B (RhB) and 4-nitrophenol (4-NP) were studied. It was assessed to verify their distinct inhibition effect on the dye treatment induced by the electron-transfer degradation processes completely.

In a typical synthesis of biocatalysts (FePd, FePdCo, PdCoCu), the biocatalysts were synthesized through "*in situ*" reduction processes. The surfactants of glutathione (GSH) and cysteine (Cys) were mediated with metal ions through the cross linkage treatment due to their functional groups (Fig. S1 ESI†). The aggregation of metal atoms was integrated together under the same experimental conditions. Metal ions (Pd^{2+}, Fe^{2+}, Cu^{2+}, Co^{2+}) were reduced, and Pd could first be reduced in an atom template form. There was a continuous deposition on the Pd atom surface, followed by a simultaneous mutual diffusion process among metal atoms. The continuous changes in the colloidal solution imply a gradual process for the mutual

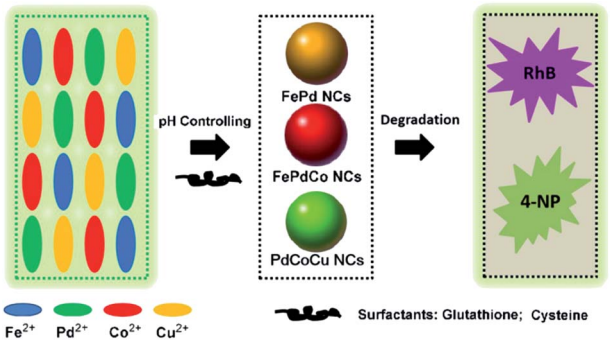

Fig. 1 Schematic of the synthetic approach of pure-phased palladium-based alloys with different surfactants (cysteine and glutathione).

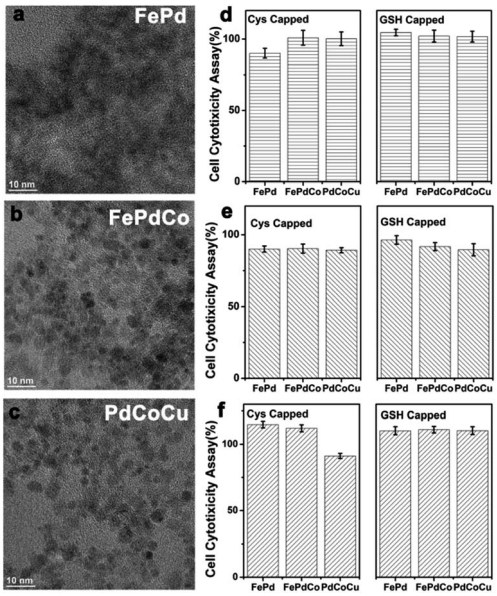

Fig. 2 Representative TEM images of GSH capped (a) FePd, (b) FePdCo and (c) PdCoCu biocatalysts. (d)–(f) Cell cytotoxicity assay (L929 cells) about Cys-/GSH-capped biocatalyst.

diffusion, and it implied that the diffusion was at the equilibrium level. The structural evolution of the alloying process was also reflected by the color change of the dispersion. GSH and Cys were treated as surfactants in order to form stable colloidal solutions. As shown in Fig. 2, it showed an ultrasmall size distribution (≤5 nm) with SPh characteristic. The sizes of FePd, FePdCo, and PdCoCu NCs were 2.77 ± 0.3 nm (based on 157 counts), 3.17 ± 0.2 nm (158 counts) and 3.33 ± 0.2 nm (178 counts), respectively as shown in Fig. S2.† To understand the synthetic procedures, Pd atoms were integrated with Fe, Co, and Cu atoms under the BH_4^- treatment.

The chemical potential of each metal ions was transferred into pure-phased metal materials due to the ion reduction procedures and alloyed diffusion mechanisms.[7] From these results, it can be seen that FePdCu NCs and PdCuCo NCs exhibit good crystallinity and size distribution; however, when using GSH as a capping surfactant, it is obviously observed that resulted size of NCs showed GSH capped NCs are much bigger than Cys capped NCs (Fig. S3 and S4 ESI†). From this phenomenon, it could be ascribed to the ligand induction, while in crystal growth, the meal atoms were aggregated together for crystalline fabrications.[8] It implied that alloys' crystallinity was improved when Pd was integrated with Fe, Co and Co, Cu, respectively. During the experiment, the dispersion was faint yellow, similarly as metal cation dispersions. The resulted colloidal solution showed dark-brown without any annealing operations. It indicated the diffusion of metal atoms into the Pd template. In addition, the zeta potential values of each biocatalyst indicated that these NCs maintained their high stability even in different solvents and after long time periods (Fig. S5 ESI†). The difference in zeta potentials can be ascribed to the ionization of functional groups (–SH, $–NH_2$, –COOH) in the alloys' structure.

The covalent linkages in two different surfactants and modified biocatalysts were confirmed by FT-IR spectroscopy (Fig. S6 ESI†). The vibrational bands of the –COOH, $-NH_2$, and –SH groups are observed at 1751, 3317, and 2520 cm^{-1}, respectively. For pure Cys and GSH, an absorption band attributable to the stretching vibration of the main alkyl chains of the surfactant is observed at 2890 cm^{-1} in the spectra of the surfactants. The absence of distinct IR peaks corresponding to the –SH group at 2520 cm^{-1} in the FT-IR spectra indicated that GSH and Cys were linked to the biocatalysts. By using BH_4^- as a reducing agent, the metal cation keeps same and unconverted consume, and the diffusion induced a large number of vacancies and voids in biocatalysts; thus, the facilitated alloy formation was solid.[9] The SPh of each alloyed Pd-formation maintained extreme stability even long time-run, reaching to a one month storing at RT.

To explore the cytotoxicity of the Cys- and GSH-capped biocatalysts at different concentrations, L929 cells were cultured in 96-well plates at a density of 5.0×10^3 cells per well for 24 h. The culture medium containing two types Cys and GSH-FePd, and FePdCo and PdCoCu colloidal solutions of the same concentrations (0.39 mg. mL^{-1}) was added to replace the original medium. These cells were cultured continuously for additional 1, 2 and 3 days. Then, the cell viability was evaluated *via* a Cell Counting Kit 8 (CCK8) following the manufacturer's instructions, as shown in Fig. 2d–f. The cell viability in the presence of six types of modified alloys (Cys and GSH capped) exhibited an excellent adaptation to various cells during 3 days of cultivation time. In fact, the cell exhibited >80% relative viability at concentrations of up to 0.39 mg. mL^{-1}, and it indicated good biocompatibility. So, the resulted alloys can be considered as nontoxic biocatalysts owing to the nature of the simple chemical modification.[10] Therefore, these modified biocatalysts constituted nontoxic candidates for cell lines. As characterized in the cell cytotoxicity assay, these alloys could exhibit good biocompatibility for further applications.

Additionally, thermogravimetric analysis (TGA) was performed for GSH- and Cys-capped alloys in the heating rate range from RT to 850 °C (Fig. S7 ESI†). These alloys could be considered as useful biocatalysts. The weight percentages of organic moieties in GSH- and Cys-biocatalysts were determined and dissolved under a thermal treatment. For GSH-capped biocatalysts, a major mass loss of 7.3% occurred between 67 °C and 230 °C, while Cys-capped biocatalysts showed a major mass loss of 4.8% from 70 °C to 220 °C. The two-stage loss of mass for each type of biocatalysts was explained by the evaporation of water and ligand decomposition processes, with the corresponding temperatures being at different stages. It might be more stable and highly crystalline while using GSH as a surfactant in the synthetic processes (*in situ* reduction).[11] So, in preparing biocatalyst, GSH-FePd was more stable than Cys-FePd NCs under same TGA measurement. As for the FePdCo biocatalysts, it showed the same tendency in the measurement, implying that the crystallinity of NCs was improved while Co doped FePd in synthetic works. The same phenomenon was also exhibited in the PdCoCu treatment. This phenomenon can be ascribed to alloyed procedure in metal atom aggregation, and it may promote the crystallinity of alloy crystals while in metal doping approaches. In addition, it also illustrated that the active spot of GSH and Cys mainly influenced the final combination while metal atom aggregated together in form of alloys.[12] It indicated the synthesis of ultrasmall palladium-based alloys (FePd, FePdCo, PdCoCu NCs) by *in situ* interactions.

As shown in Fig. 3, the crystal phase changed as in the reflection of X-ray diffraction (XRD) patterns, Pd-based bimetallic FePd NCs and ternary FePdCo, PdCoCu alloys can be well measured and defined the integration of Fe, Pd, Co, Cu elements. It revealed that the intensity of the XRD pattern of each biocatalyst is subjected to the growth process and crystalline characterization because it is closely related to the catalytic activity of biocatalysts in "electron–hole" applications. According to the wide-angle XRD patterns (Fig. 3a and S8 ESI†), we found that the introduction of these biocatalysts has much higher intensity and crystallinity when capped by GSH rather than Cys modified, and it can be attributed to the $E_{interaction}$ of GSH and Cys calculated to be −86.48 and −45.82, respectively. The mentioned negative values suggested that the surfactant molecules interacted with metal species, and the final fabrication achieved high crystallinity.

As shown, it illustrated the (1, 1, 1), (1, 1, 0), (2, 0, 0), and (2, 2, 0) lattice response peaks exactly. Doping metal elements in synthesis processes even changed the capped molecules, which proved that the crystalline growth had metal elements dopping. Same as the XRD characterization of GSH-capped biocatalysts, Cys-capped NCs corresponded with XRD illustration (Fig. S8 ESI†). Clearly, it revealed that high-mass molecules could cross-link with metal species, and the final fabrication achieved higher crystallinity. These biocatalysts showed a common fcc structure, and the relative intensity of the diffraction peaks of ternary NCs (FePdCo, PdCoCu) increased with the metal element doping. It indicated the success in fabricating the alloys. The broadened diffraction peaks from alloys indicated small crystal grain sizes of FePd. However, ternary FePdCo and PdCoCu NCs had bigger size (FePd < FePdCo < PdCoCu). The calculation about the size distributions of NCs was done from the (1, 1, 1) and (1, 1, 0) peaks by using the Scherrer's formula. Fig. 3b shows the fabrication process of FePd, FePdCo, PdCoCul alloys. Due to the difference in the chemical potential of

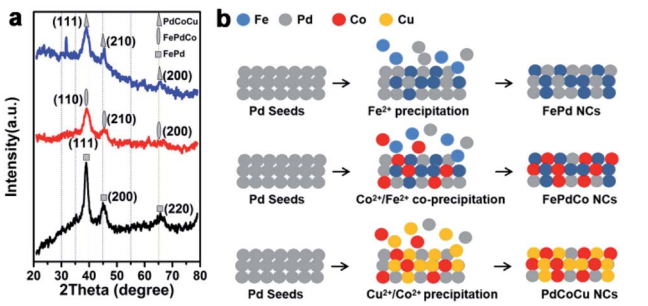

Fig. 3 (a) Powder XRD characterization of GSH capped biocatalysts: FePd, FePdCo and PdCoCu biocatalysts. (b) Schematic conversion about metal atom based solid-state transmissions in synthetic procedures in palladium-based alloyed biocatalysts.

different elements, Pd (2.20) exhibited much higher electronegativity than Fe, Co, Cu elements, and thus the formation of alloyed biocatalysts enabled electron transfer among the metal atoms, which contributed to the hybridization of metals. It obviously indicated that Pd was first achieved as seeds in processing the alloyed biocatalysts. Among the co-precipitation about Fe, Co, Cu metal elements on Pd surface, it maintained at initial growth stage from nuclei to crystalline appearance.[13] The following culturing in the crystalline growth showed that the necessary limitation towards size and structural uniformity referred to their higher crystalline and improved properties. Due to of SPh characteristic, these biocatalysts should be fabricated in water-based mediums underwent *in situ* growth mechanism at RT. In which, it was less exhaust and simple operation than hydrothermal or solvothermal approaches exhibited. Eventually, the ultrasmall size distribution offered a high surface area and relative catalytic activity in water-phased media without adding any carbon modification or loads.

Among current studies on common organic materials, the target conducting molecules could act as landmark degraders and serve as test catalytic properties. It could be visualized by the colour changes and characteristic peak in the UV spectrum along with time. The catalytic activities of biocatalysts were evaluated by reducing RhB and 4-NP molecules with excess $NaBH_4$. As Pd (2.20) has much higher electronegativity, biocatalysts enabled electron transfer among the metal atoms, which could contribute to the hybridization of metals. Notably, the catalytic activity of GSH-capped FePd, FePdCo and PdCoCu alloys were higher than that of Cys-capped biocatalysts. The catalytic performance of both GSH- and Cys-capped biocatalysts could be attributed to the monodispersed state, ultrasmall size distribution and SPh characteristic, which facilitated a large reaction area and possessed a great number of active reduction sites, thereby accelerating the reaction *via* a facile adsorption of BH_4^- donors.[14] Fig. 4a–f show the UV-vis spectra acquired during the reduction of 4-NP and RhB with $NaBH_4$ in the presence of GSH-capped alloys (FePd, FePdCo, PdCoCu) at a loading of 1.5 mg. The intensity of the 4-NP absorbance band decreases within 6 min after the addition of $NaBH_4$. PdCoCu NCs have a weaker reduction ability and require 10 min for the degradation of 4-NP molecules (Fig. 4a–c). As appeared in the reduction process, the ability of GSH-capped alloyed NCs exhibited higher catalytic capacity than Cys-capped NCs. The most immediate reason is the difference in crystallinity. In addition, the intensity of the RhB absorbance band decreased when the initial stage disappeared completely within 2 min (Fig. 4d–f). It proved that these biocatalysts exhibited high catalytic performance under mild conditions, which indicated the efficient charge transfer for cascade-type catalytic reactions. The degradation efficiency was estimated with GSH- and Cys-capped NCs (Fig. 4g–i, S9 and S10 ESI†). As time passed, the solution phase finally became transparent, which implied that the degradation finished completely.

Evidently, it introduced the higher degradation efficiency in RhB within 2 min when GSH-capped alloys were used, and the longer time consuming appeared in Cys-capped biocatalyst reductions. This discrimination revealed that the catalytic effect of GSH-capped biocatalysts was clearly distinguishable in the reduction reaction. Compared in crystalline characteristics in TEM characterizations, the lower crystalline was achieved while using Cys as surfactant in synthesized works, which corresponded with this feature and implied the relative lower

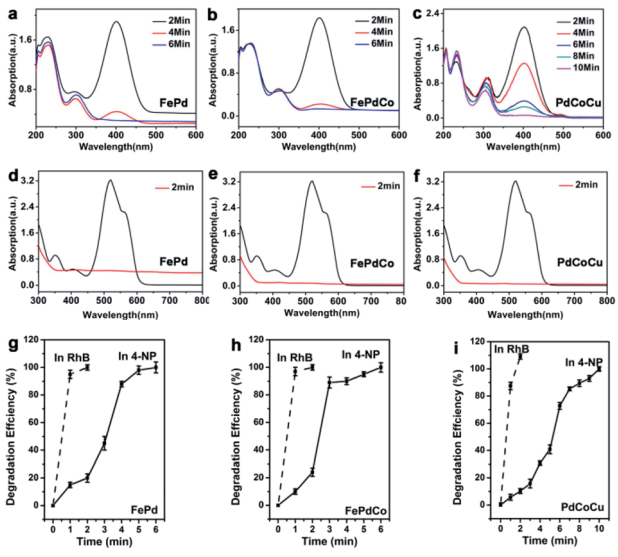

Fig. 4 Representative catalytic properties of GSH-capped biocatalysts. The UV-Vis spectra acquired during the reduction of 4-NP and RhB at different reaction intervals employing (a) and (d) FePd, (b) and (e) FePdCo and (c) and (f) PdCoCu NCs as the catalysts. (g)–(i) Degradation efficiency of FePd, FePdCo and PdCoCu alloys at RT.

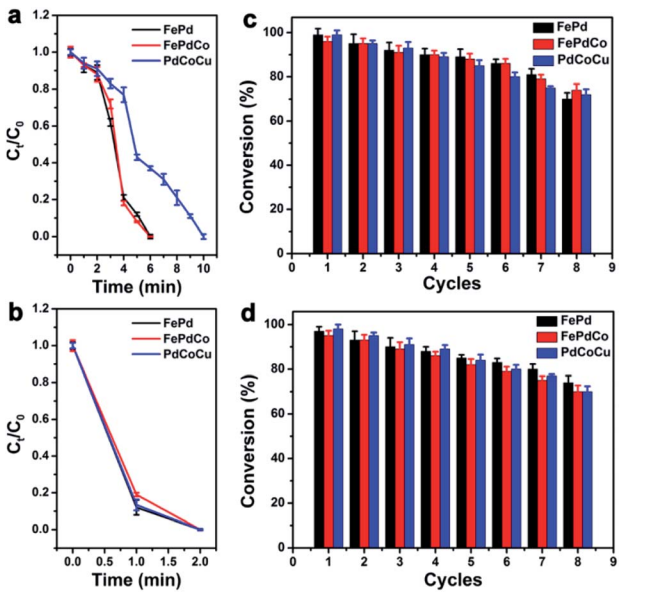

Fig. 5 (a) and (b) GSH-capped biocatalysts (FePd, FePdCo and PdCoCu), the C_t/C_0 ratio was calculated from the relative 4-NP absorption value at 400 nm and RhB molecules at 553 nm, respectively. (c) and (d) Reusability of GSH-capped biocatalysts (FePd, FePdCo and PdCoCu) that were retrieved by centrifugation after multiple reduction cycles.

catalytic performance. It also demonstrated the relationship between catalytic performance and alloys' crystallinity.[15] Furthermore, the absorption peaks at 400 nm and 553 nm were obtained corresponding to 4-NP and RhB, respectively, which are colourless in their reduced leuco forms. Plots of C_t/C_0 depending on time for the reduction of 4-NP and RhB in the presence of biocatalyts were obtained, and the C_t/C_0 ratio was calculated from the relative equation (Fig. 5a and b, illustration in ESI†).[16] The faster degradation of the target molecules occurred at a higher loading of both GSH- or Cys-capped biocatalysts. After adding the biocatalysts, the absorption value at 400 nm (4-NP) and 553 nm (RhB) decreased with the progression of the reaction. The recyclability of the biocatalysts was also investigated (Fig. 5c and d). The recyclable utilization of biocatalysts demonstrated durable stability even after 8 reduction cycles, and the conversion still remained above 70% level. The larger decrease in the catalytic activity of Cys-capped biocatalysts following each reduction cycle compared with that of GSH-capped biocatalysts was due to the weaker crystalline degree than the Cys-modified biocatalysts.

Conclusions

In summary, a feasible alloying strategy is proposed at RT environment and verified experimentally to clearly enhance the performance of biocatalysts towards the RhB and 4-NP in water-soluble media. Its ultra-smaller and SPh properties offered higher convenience in catalytic measurements. It gave higher affinity between target and catalysts, and the ultrasmall size offered a higher surface area. By using Cys and GSH as surfactants for synthesizing biocatalysts, it showed a common phenomenon in the crystalline growth and high catalytic activity. The resulted biocatalysts were one kind of unique electrocatalysts, which are active, selective and robust to catalyze the organic dyes in water-soluble media. The demonstrated alloying strategy in this study could be adaptable to concurrently improve the conversion efficiency and selectivity of other hydrogenation reactions. These alloys having higher biocompatibility could potentially be applied as recyclable metal-based functional catalysts. Furthermore, the requirements about novel applications such as peroxidase-mimicking enzymes, anti-oxidizing agents, and biosensors should be considered as the advancement in merged catalytic and biological applications.

Methods/experimental

All experimental details for this study are available in the ESI.†

Conflicts of interest

There are no conflicts to declare.

Acknowledgements

This work was supported by the Science and Technology Research program of Chongqing Municipal Education Commission (Grants no. KJQN201900436, KJQN202000420), the Science and Technology Planning Project of Yuzhong District, Chongqing, China (Grants no: 20200118) and the Special Funds for Technology Innovation and Application Development of Chongqing, China (Grants no: cstc2020jscx-msxmX0064).

References

1 (*a*) T. Yang, L. Wei, L. Jing, J. Liang, X. Zhang, M. Tang, M. J. Monteiro, Y. I. Chen, Y. Wang and S. Gu, *Angew. Chem., Int. Ed.*, 2017, **56**, 8459–8463; (*b*) T. Matsuno, S. Kamata, S. Sato, A. Yokoyama, P. Sarkar and H. Isobe, *Angew. Chem., Int. Ed.*, 2017, **129**, 15020–15024; (*c*) Y. Lee, M. A. Garcia, N. Freyhuls and S. Sun, *Angew. Chem., Int. Ed.*, 2010, **49**, 1271–1274; (*d*) S. Lee and Y. M. Chung, *Catal. Today*, 2019, **352**, 270–278; (*e*) J. Wu, G. G. Chang, Y. Q. Peng, X. C. Ma, S. C. Ke, S. M. Wu, Y. X. Xiao, G. Tian, T. Xia and X. Y. Yang, *Chem. Commun.*, 2020, **56**, 6297–6300; (*f*) S. Xie, M. Jin, J. Tao, Y. Wang, Z. Xie, Y. Zhu and Y. Xia, *Chem.–Eur. J.*, 2012, **18**, 14974–14980; (*g*) H. Nan, Y. Q. Su, C. Tang, R. Cao and X. Tian, *Sci. Bull.*, 2020, **65**, 1396–1404.

2 (*a*) J. Kwon, X. Mao and J. Lee, *Curr. Appl. Phys.*, 2017, **17**, 1066–1078; (*b*) D. Wang and Y. Li, *Adv. Mater.*, 2015, **23**, 1044–1060; (*c*) Y. Hou, H. Kondoh, T. Kogure and T. Ohta, *Chem. Mater.*, 2004, **16**, 11750–11758; (*d*) S. Guo, S. Zhang, X. Sun and S. Sun, *J. Am. Chem. Soc.*, 2011, **133**, 15354–15357; (*e*) N. H. Luong, T. T. Trung, T. P. Loan, L. M. Kien, T. T. Hong and N. H. Nam, *J. Electron. Mater.*, 2016, **45**, 4309–4313.

3 (*a*) S. G. Vermilyea, Z. Cai, W. A. Brantley and J. C. Mitchell, *Int. J. Prosthodont.*, 1996, **5**, 288–294; (*b*) D. Sun, W. A. Brantley, R. H. Heshmati and W. M. Johnston, *Sensors*, 2020, **3**, 1–5; (*c*) H. Wu, X. Zuo, Y. Wang, K. Zhang and Y. Chen, *Adv. Mater. Res.*, 2014, **1028**, 14–19.

4 (*a*) Z. Yan, M. G. Taylor, A. Mascareno and G. Mpourmpakis, *Nano Lett.*, 2018, **18**, 2696–2704; (*b*) E. K. Fox, F. E. Haddassi, J. Hierrezuelo, T. Ninjbadgar, J. K. Stolarczyk, J. Merlin and D. F. Brougham, *Small*, 2018, **14**, 1802278; (*c*) W. Heni, L. Vonna and H. Haidara, *Nano Lett.*, 2015, **15**, 442–449.

5 (*a*) W. Xu, M. Wang, Z. Li, X. Wang, Y. Wang, M. Xing and Y. Yin, *Nano Lett.*, 2017, **17**, 2713–2718; (*b*) Y. Liu, D. L. Purich, C. Wu, W. Yuan, T. Chen, C. Cui, L. Zhang, S. Cansiz, W. Hou and Y. Wang, *J. Am. Chem. Soc.*, 2015, **137**, 14952–14958; (*c*) T. Zhang, J. Ge, Y. Hu and Y. Yin, *Nano Lett.*, 2007, **7**, 3203–3207.

6 (*a*) Y. Ding, F. Fan, Z. Tian and Z. L. Wang, *J. Am. Chem. Soc.*, 2010, **132**, 12480–12486; (*b*) C. D. Fuerst and E. G. Brewer, *Appl. Phys. Lett.*, 1990, **56**, 2252–2254.

7 H. Zhu, S. Zhang, D. Su, G. Jiang and S. Sun, *Small*, 2015, **11**, 3545–3549.

8 M. Sawczyk and R. Klajn, *J. Am. Chem. Soc.*, 2017, **139**, 17973–17978.

9 J. Kwon, X. Mao, H. Lee, S. Oh, L. Tufa, J. Choi, J. Kim, C. Kim, J. Kim, D. Hwang and J. Lee, *J. Colloid Interface Sci.*, 2021, **588**, 646–656.

10 (*a*) D. Wang and D. Astruc, *Chem. Rev.*, 2014, **114**, 6949–6985; (*b*) H. Zhou, I. C. Sun, F. Zou, S. Oh and J. Lee, *ACS Appl. Mater. Interfaces*, 2014, **6**, 19680–19689.

11 H. A. Vankalkeren, S. L EeNders, C. Hommersom, F. Rutjes and F. L. Vandelft, *Chem.–Eur. J.*, 2011, **17**, 11290–11295.

12 (*a*) F. Liu, W. Lou, J. Wang, Q. Li and W. Shen, *Plant Physiol. Biochem.*, 2021, **167**, 68–76; (*b*) S. Li, S. Guo, H. Yang, G. Guo, R. Ren, J. Li, Z. Dong, J. Jin and J. Ma, *J. Hazard. Mater.*, 2014, **270**, 11–17.

13 (*a*) Y. Xia, X. Xia and H. C. Peng, *J. Am. Chem. Soc.*, 2015, **46**, 7947–7966; (*b*) C. Tan and Z. Hua, *J. Am. Chem. Soc.*, 2016, **46**, 12162–12174; (*c*) X. Chen, X. J. Li, Y. Huang, J. Wei and N. Zheng, *Biomater. Sci.*, 2017, **5**, 2448–2455.

14 (*a*) S. Zhang, S. Gai, F. He, S. Ding, L. Li and P. Yang, *Nanoscale*, 2014, **6**, 11181–11188; (*b*) H. Yang, S. Li, X. Zhang, X. Wang and J. Ma, *J. Mater. Chem. A*, 2014, **2**(30), 12060–12067.

15 (*a*) Y. Li, Y. Yu, Y. Huang, R. A. Nielsen, W. A. Goddard, Y. Li and L. Cao, *ACS Catal.*, 2015, **5**, 448–455; (*b*) F. Liu, K. Huang, A. Zheng, F. S. Xiao and S. Dai, *ACS Catal.*, 2017, **8**, 372–391; (*c*) J. Li, H. Liu, J. Ming, D. Sun, X. Chen, X. Liu and N. Zheng, *Chem. Sci.*, 2019, **10**, 1677–1686.

16 (*a*) T. Wu, G. Liu, J. Zhao, H. Hidaka and N. Serpone, *J. Phys. Chem. B*, 1998, **102**, 5845–5851; (*b*) C. Singh, A. Goyal and S. Singhal, *Nanoscale*, 2014, **6**, 7959–7970.